Energy Conversion and Management 252 (2022) 115074

Contents lists available at ScienceDirect

Energy Conversion and Management

journal homepage: www.elsevier.com/locate/enconman

A novel lung-inspired 3D-printed desiccant-coated heat exchanger for high-performance humidity management in buildings

Umamaheswar Puttur [1], Masoud Ahmadi [1], Behzad Ahmadi, Sajjad Bigham [*]

Department of Mechanical Engineering-Engineering Mechanics, Michigan Technological University, 1400 Townsend Drive, Houghton, MI 49931-1295, USA

ARTICLE INFO

Keywords:
Dehumidification
Desiccant-coated heat exchanger
Lung-inspired 3D-printed heat exchanger
Solid desiccant
Intertwined bicontinuous flow network

ABSTRACT

Offering an independent humidity management method for buildings, desiccant-coated heat exchangers (DCHXs) are deemed a promising approach to improve the overall energy efficiency of air conditioning (AC) systems. State-of-the-art DCHXs, however, are bound with conventional HX topologies either providing limited desiccant-air interfacial areas or introducing excessive pressure drop penalties. Here, a novel 3D-printed DCHX concept inspired by the bronchi arrangement of a human lung is introduced to address the shortcomings inherent in existing DCHX designs. The proposed lung-inspired DCHX utilizes two intertwined bicontinuous flow networks enabling highly efficient heat and mass transfer characteristics for augmented adsorption and regeneration processes at low pressure drop penalties. While the first network evenly distributes an incoming air stream through the entire volume of the lung-inspired DCHX, the second network volumetrically splits a cooling water stream within and through the first network. Effects of various parameters including air flow rate, outdoor air humidity ratio, and regeneration temperature on dehumidification performance and energy efficiency of the proposed lung-inspired DCHX were investigated. Experimental results indicated the proposed lung-inspired 3D-printed DCHX outperforms existing DCHX systems by demonstrating an excellent balance between a high volumetric adsorption rate and a low pressure drop penalty. The volumetric adsorption rate of the proposed lung-inspired DCHX technology is 54.8 g/m^3-s, a more than two-fold improvement compared with state-of-the-art DCHX systems. Additionally, the lung-inspired DCHX offers high thermal energy efficiency of 56% at a low regeneration temperature of 40 °C. Therefore, the proposed lung-inspired 3D-printed DCHX offers a new solid-desiccant-based air dehumidification pathway for next-generation high-performance AC systems.

1. Introduction

Global demand for energy-efficient air conditioning (AC) systems is boosting due to rising consumer awareness over energy efficiency, growing energy bills, and climate change concerns. Buildings' latent cooling (i.e., humidity) load can account for up to 85% of total AC energy consumption in mixed-humid and hot-humid climate zones [1]. While the latent cooling load is a key contributor to the overall AC demand, existing vapor-compression-based AC technologies cannot efficiently treat humidity since latent and sensible cooling loads are highly coupled in current systems [37]. Therefore, effective and/or independent humidity management [37–39] is a key concept to the development of future energy-efficient AC systems.

A solid-desiccant-based dehumidification system offers a promising approach to independently manage latent cooling load, thereby boosting the energy efficiency of AC systems. Here, the air humidity is adsorbed by a hygroscopic solid-desiccant material demonstrating a natural tendency toward water vapor. Fixed packed solid-desiccant beds are common dehumidification systems for compressed air and pressurized process gasses [2–5]. They typically consist of two packed towers for sorption and regeneration processes enabling a continuous dehumidification operation. The process air flows through the first packed bed and gets dehumidified. Once the first bed is saturated with moisture, the process air is directed to the second desiccant bed, and the first bed is regenerated by a hot air stream. In other words, the process air is switched between the two desiccant beds at a predetermined cycling time depending on the size of the system and its thermo-hydraulic characteristics. Recently, Shamim et al. [6] studied a multilayer fixed-bed binder-free desiccant air dehumidifier for air-conditioning systems. Silica-based high-purity spherical gels fixed in metal meshes that

* Corresponding author.
E-mail address: sbigham@mtu.edu (S. Bigham).
[1] Equal contribution.

https://doi.org/10.1016/j.enconman.2021.115074
Received 2 October 2021; Received in revised form 4 November 2021; Accepted 26 November 2021

eliminate polymer binders were employed as adsorbents. Compared with conventional desiccant dehumidification systems, they observed a significant reduction in pressure drop and a boost in dehumidification capacity due to the high adsorption capacity of silica gels. Packed desiccant bed systems, however, are bulky requiring a large footprint area due to a low moisture removal rate [3]. Furthermore, the packed desiccant-bed towers introduce high air pressure drop penalties, thereby increasing the overall energy consumption of the system.

The moisture removal performance of fixed packed desiccant beds can be improved through a desiccant wheel dehumidifier offering a continuous operation and thus eliminating switching flow control valves. A desiccant wheel comprises a honeycomb structure impregnated with or entirely fabricated from a solid desiccant medium. The wheel slowly rotates at a speed of 10 to 30 rotations per hour. While a section of the wheel adsorbs the humidity of the incoming outdoor air stream, the other section of the wheel simultaneously undergoes the regeneration process facilitated by a hot air stream [7]. Therefore, a desiccant wheel allows a continuous dehumidification operation without requiring a complex control system. Zhou et al. [8] proposed a non-adiabatic internally-cooled desiccant wheel to enable a quasi-isothermal dehumidification process. Compared to a tube-shell design, the proposed wheel did not have multiple desiccant layers overlapping each other, thereby avoiding a high heat resistance. The enthalpy effectiveness of the non-adiabatic wheel was on average 11% higher than that of conventional desiccant wheels under a wet performance mode. Goldsworthy et al. [9] investigated limiting mechanisms in desiccant rotary wheel dehumidifiers. They concluded that the adsorption process is primarily limited by the exothermic heat generated during the adsorption process. Heat carryover from the regeneration section to the adsorption segment has been also identified to additionally hinder the dehumidification rate and overall energy performance of the system [10–14].

To overcome the heat carryover issue, a fluidized bed concept has been proposed as an alternative to the desiccant wheel dehumidifiers. A fluidized bed consists of suspended desiccant particles flying through a pressurized incoming humid air. Here, active desiccant particles capture air moisture, thereby dehumidifying the humid air stream. Chen et al. [15] proposed a circulating fluidized system employing two beds for adsorption and regeneration processes. Suspended desiccant particles were continuously switched between the adsorption and regeneration fluidized beds through two connecting channels, thereby enabling a continuous dehumidification operation. Compared with a packed bed dehumidifier, a circulating fluidized bed system with vertical connecting tubes showed a 22% improvement in dehumidification rate [16]. Fluidized bed dehumidification systems, however, employ suspended desiccant particles undergoing continuous collisions between desiccant particles and with the wall boundaries of the system. The result is a fine dust formation in the supply air stream. This makes a fluidized bed dehumidifier largely inappropriate for most air conditioning applications.

Several challenges associated with the above solid-desiccant-based dehumidifier systems including limited heat and mass transfer characteristics, regeneration heat carryover, and dust formation could be potentially addressed by a desiccant-coated heat exchanger (DCHX) concept. The main idea of a DCHX module is to use a conventional heat exchanger system coated with a solid-desiccant material. A DCHX is ideal for dehumidification applications as the heat generated during the adsorption process could be effectively dissipated through its embedded cooling channels. Consequently, the development of efficient DCHX-based dehumidification systems has recently gained increased attention [17–25]. Existing DCHX designs mostly utilize fin-tube and/or other simple heat exchanger topologies [27–34]. Vivekh et al. [32] conducted a comprehensive review of recent developments in DCHXs and summarized parameters affecting the performance of DCHX systems including inlet air flow rate, air flow temperature, inlet air relative humidity, and internal cooling. Recent attempts have mainly focused on improving the performance of DCHX systems through novel composite desiccants. For instance, superabsorbent polymers and potassium format coated heat exchangers were investigated and found to have an almost 3–4 times higher sorption capacity than pure/composted silica gel-based DCHXs [33]. Mohammed et al. [34] compared the performance of a silica gel aluminum foam heat exchanger and a desiccant packed heat exchanger. They showed that the desiccant packed heat exchanger outperforms the silica gel aluminum foam heat exchanger due to its higher moisture removal ability and higher density of the desiccant material. More recently, Wang et al. [35] examined the dehumidification performance of a desiccant-coated microchannel heat exchanger. The surface of the heat exchanger was coated with type B silica gel using an electrostatic powder spray. They reported that the heat and moisture transfer coefficients increase at smaller hydraulic diameters (i.e., smaller fin pitches). Additionally, the air mass flow rate was recognized as the most influential parameter affecting dehumidification performance. However, current DCHXs are bound with conventional HX topologies that either provide a limited desiccant-air interfacial area in the case of fin-tube HXs or introduce excessive pressure drop penalties in the case of packed and foam DCHX units.

Here, a novel lung-inspired 3D-printed DCHX is introduced to address the shortcomings associated with conventional DCHXs. The proposed lung-inspired DCHX utilizes two intertwined bicontinuous flow networks for the air and cooling water streams to provide desirable heat and mass transfer characteristics at a low pressure drop penalty. In the following sections, first, the proposed DCHX concept is introduced. Next, the 3D-printing and desiccant coating approaches are discussed. Then, the dehumidification test setup facility is explained. Finally, adiabatic/diabatic adsorption and regeneration characteristics of the lung-inspired 3D-printed DCHX are examined.

2. Concept: lung-inspired desiccant-coated heat exchanger

Next-generation high-performance solid-desiccant-based dehumidification systems demand highly efficient heat and mass transfer characteristics boosting adsorption and regeneration processes at low pressure drop penalties. This requires novel dehumidifier architectures employing complex features and flow distribution pathways with amplified desiccant-air interfacial areas. This is now possible owing to recent advancements in modern manufacturing techniques including 3D printing.

The proposed 3D-printed DCHX design is inspired by the bronchi arrangement of a human lung demonstrating an improved flow distribution for highly efficient heat and mass exchange rates. Detailed schematics of the proposed lung-inspired 3D-printed DCHX are shown in Fig. 1. Fig. 1d shows a cell-level unit that was employed as a base structure for the lung-inspired DCHX module. Each cell has three converging inlet pathways and three diverging outlets each of which at a different 3D spatial orientation. As shown, the proposed architecture utilizes two intertwined bicontinuous flow networks for desirable heat and mass transfer characteristics at a low pressure drop penalty. The first network (i.e., the sandcastle color in Fig. 1b and c) evenly distributes an incoming air stream through the entire volume of the DCHX. The second network (i.e., the blue color in Fig. 1b and c) volumetrically splits the cooling water within and through the first network. To enable the desiccant-based dehumidification process, the surface of the air network is coated with a desiccant material. The desiccant coating allows mass transfer between an incoming humid air stream and the desiccant material.

Fig. 2 shows schematics of the heat and mass transfer events present in the proposed lung-inspired 3D-printed DCHX concept during the adsorption and regeneration processes. During the adsorption process (cf. Fig. 2a), the humidity of an incoming moist air stream is captured by the active desiccant-coated layer. The adsorption process is a mass transfer event governed by the water vapor pressure potential (i.e., the difference between the partial water vapor pressure of the air stream and

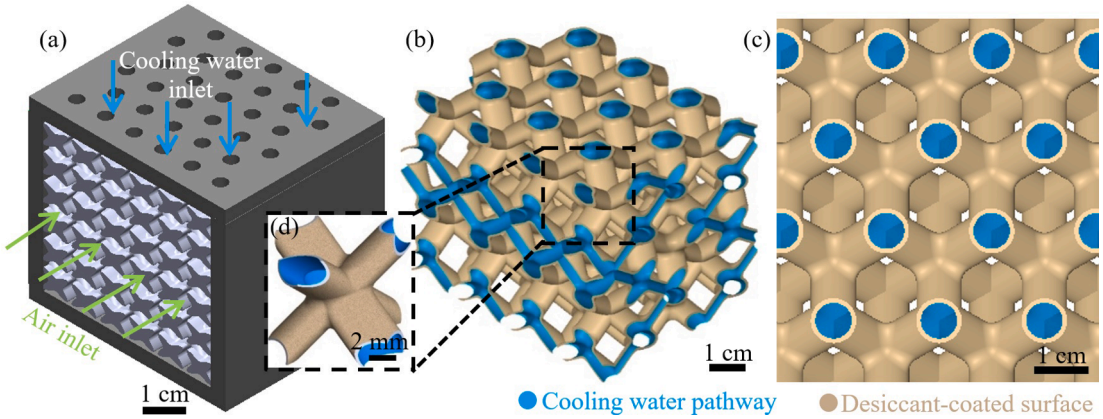

Fig. 1. Detailed schematics of the proposed lung-inspired 3D-printed DCHX: (a) an overall 3D model, (b) a 3D view of the two intertwined bicontinuous flow networks, (c) a 2D cross-sectional view, and (d) a single cell-level structure.

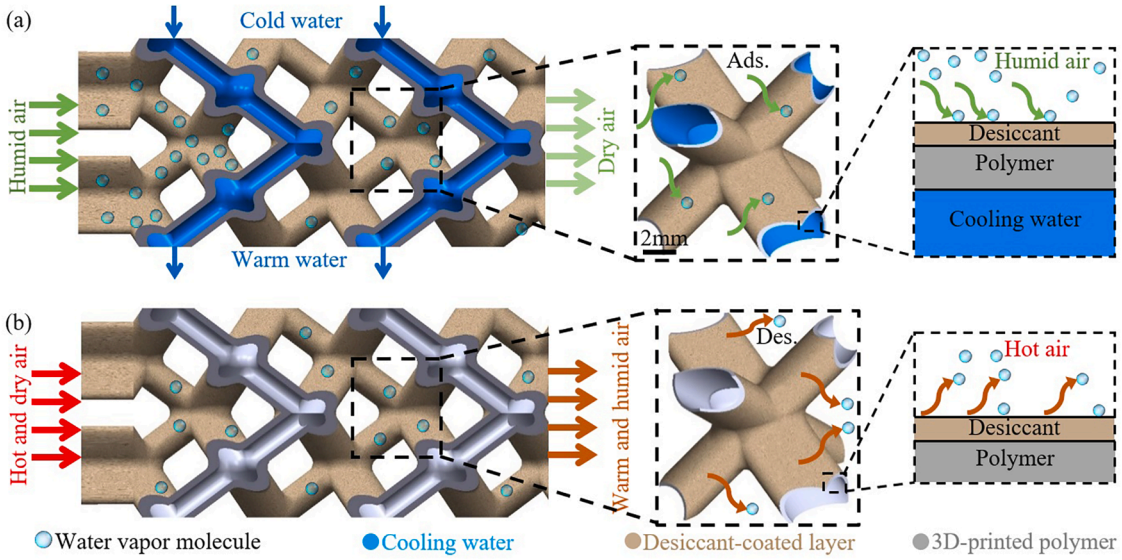

Fig. 2. Schematics of the heat and mass transfer events present in the proposed lung-inspired 3D-printed DCHX concept during the (a) adsorption, and (b) regeneration processes.

the equilibrium water vapor pressure at the desiccant-air interface). This process is an exothermic reaction releasing the adsorption heat at the desiccant-coated layer. The adsorption heat is dissipated partly by the incoming air stream and largely by the cooling water stream flowing through the liquid network. The chilled water stream cools the solid desiccant layer, thereby decreasing its equilibrium water vapor pressure. This subsequently improves the adsorption rate. Once saturated with humidity, the solid desiccant layer is regenerated by a hot air stream. Similar to the adsorption process, the regeneration process (cf. Fig. 2b) is a mass transfer event governed by the water vapor pressure potential. During the regeneration process, heat is transferred to the desiccant layer increasing its equilibrium water vapor pressure. As a result, the previously adsorbed water vapor molecules are rejected from the desiccant layer, thereby resuming the water vapor capture potential of the desiccant media. This allows the lung-inspired DCHX module to be again employed for the adsorption process, thereby completing an adsorption-regeneration cycle. It should be noted that the regeneration process can be alternatively enabled by a hot liquid stream flowing through the liquid network.

The design provides an excellent contact area with a minimum thermal resistance between air, coated desiccant media, and cooling water, thereby ensuring effective heat and mass transfer characteristics at a low pressure drop penalty as key performance metrics for solid-desiccant-based dehumidification systems. As the proposed DCHX design is a monolithic structure with embedded cooling channels facilitating to dissipate the adsorption heat, the new lung-inspired 3D-printed DCHX is expected to outperform existing desiccant-based dehumidifiers.

The proposed lung-inspired 3D-printed DCHX concept is envisioned to be an integral part of a solid-desiccant-based air dehumidification system. This allows to independently manage humidity in buildings, thereby boosting the energy efficiency of AC systems. The air dehumidification system employs two dedicated lung-inspired 3D-printed DCHX modules for the adsorption and regeneration processes. While the adsorber DCHX module dehumidifies a humid air stream, a hot air stream simultaneously desorbs the captured humidity away from the coated desiccant media in the regenerator module. Once the desiccant media of the adsorber module is saturated with moisture, the two air streams are switched. This allows a continuous dehumidification process.

3. 3D-printing and desiccant coating of the lung-inspired DCHX

The proposed lung-inspired DCHX was fabricated using a

stereolithography (SLA) based 3D-printing method. The SLA method uses an ultraviolet laser beam to selectively cure a photopolymer resin. This continuously adds a new layer on top of the previously cured resin layer. The laser beam is controlled by a computer-aided design model. The finished product is then washed off with alcohol such as isopropyl alcohol (IPA) to remove the excess resin. The 3D-printed green parts are then fully hardened with an ultraviolet light source for 30 min to an hour. In this work, the SLA 3D-printer offered by Formlabs Form 3 was employed. Fig. 3a shows a 3D-printed DCHX employing a lung-inspired architecture. As shown in Fig. 3b, the 3D-printed DCHX utilizes two intertwined bicontinuous flow networks for the air and cooling water streams. The geometrical specifications of the lung-inspired 3D-printed DCHX are listed in Table 1.

The proposed dehumidifier module has a desiccant layer coated on the air-side flow stream. The desiccant material used in this study is a mixture of molecular sieves with a 4A pore diameter. This desiccant has a color indicator exhibiting two different colors when it is active or otherwise saturated. Properties of the molecular sieve selected are listed in Table 2. To prepare the desiccant slurry required for coating, the desiccant particles were initially pounded into powders using a mortar and pestle. The desiccant powder was then sieved through a copper mesh to procure a uniformly fine desiccant powder as shown in Fig. 3c.

A binder material is required to reliably adhere the desiccant powder to the air-side solid surfaces of the proposed DCHX. Li et al. [26] investigated a binder coating method and proposed different potential binder agents for various desiccant materials. They suggested the optimal binder/desiccant ratio to avoid an excessive resistance that might hinder the mass transfer process. For the current work, polyvinyl alcohol (PVA) was chosen to be the binding element due to its good adhesive abilities without introducing exacerbated heat and mass transfer resistances. The binder solution was prepared by slowly adding and constantly stirring the PVA pellets to distilled water at room temperature. The total amount of PVA added was 17 percent by weight of distilled water. Stirring was continued until no lumps were seen in the mixture as it turned to a foggy white solution. This mixture was then kept undisturbed at room temperature overnight to obtain a clear solution (cf. Fig. 3d) before using it as a binding agent.

To coat the desiccant-binder mixture on the air-side solid surfaces of the 3D-printed heat exchanger, different ratios of the above PVA-powder solution were explored. Parameters such as adherence to the surface, thermal resistance, and air flow resistance were considered. In the present experimental study, a mixture combination of 87% by weight desiccant powder and 13% by weight PVA solution was found to be optimum. The prepared solution was then taken in small amounts and deposited onto the heat exchanger air flow surfaces until the whole external features were completely coated with the desiccant solution. Once the air-side solid surfaces were completely coated with the desiccant glue, it was allowed to be dried as shown in Fig. 2e.

Table 1
Geometrical specifications of the proposed lung-inspired 3D-printed DCHX.

Parameter	Value
Cell tube diameter	4 mm
Cell wall thickness	1 mm
Pitch length	10 mm
Total number of cell structures	216
Total number of inlets/outlets	33/33
The volume of the DCHX	700 (W) × 600 (H) × 550 (L) mm^3

Table 2
Properties of the molecular sieve mixture employed.

Composition	$Na_{12}[(AlO_2)_{12}(SiO_2)_{12}]. nH_2O$
Particle size	8–12 mesh
Pore diameter	4A
Particle form	beads

4. Experimental setup and uncertainty analysis

4.1. DCHX assembly

Once the desiccant slurry was applied and dried, the lung-inspired 3D-printed DCHX was ready to be tested. Fig. 4a shows the 3D-printed DCHX with assembled inlet and outlet manifolds. A neoprene rubber lining was provided between the DCHX and manifold interfaces to prevent potential fluid leakages. Four T-type thermocouples (Model: ReoTemp F-M12T1SU4) were employed to measure air and cooling water temperatures at the inlet and outlet ports. The 3D-printed DCHX was then embedded in a dehumidification test facility.

4.2. Dehumidification test facility

Fig. 4b and c show an image and a schematic of the dehumidification test loop facility to evaluate the performance of the lung-inspired 3D-printed DCHX. As shown, the dehumidification test facility has two modes of operation. In the dehumidification mode, a humid air stream with a known temperature and relative humidity enters the DCHX module. The humidity of the incoming air stream is captured by the coated desiccant media as the humid air stream passes through the lung-inspired DCHX. Once the desiccant media are statured with humidity, the dehumidification process ceases. In the regeneration mode, a hot air stream rejects the adsorbed water vapor molecules. This activates the desiccant media for further dehumidification process. An air heater adjusts the temperature of the air stream for the regeneration process.

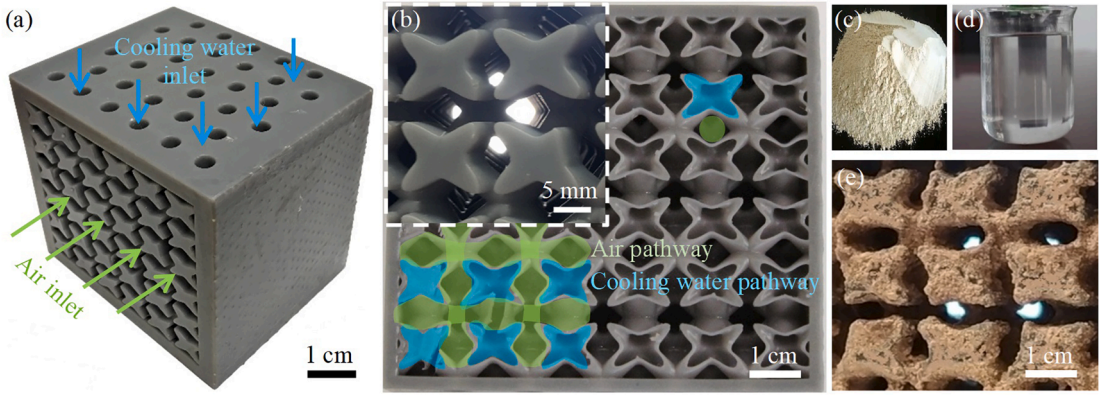

Fig. 3. The lung-inspired 3D-printed DCHX development: (a) an image of the 3D-printed DCHX, (b) a 3D view of the intertwined bicontinuous flow networks, (c) desiccant powder, (d) binder solution, and (e) an image of the desiccant-coated surface.

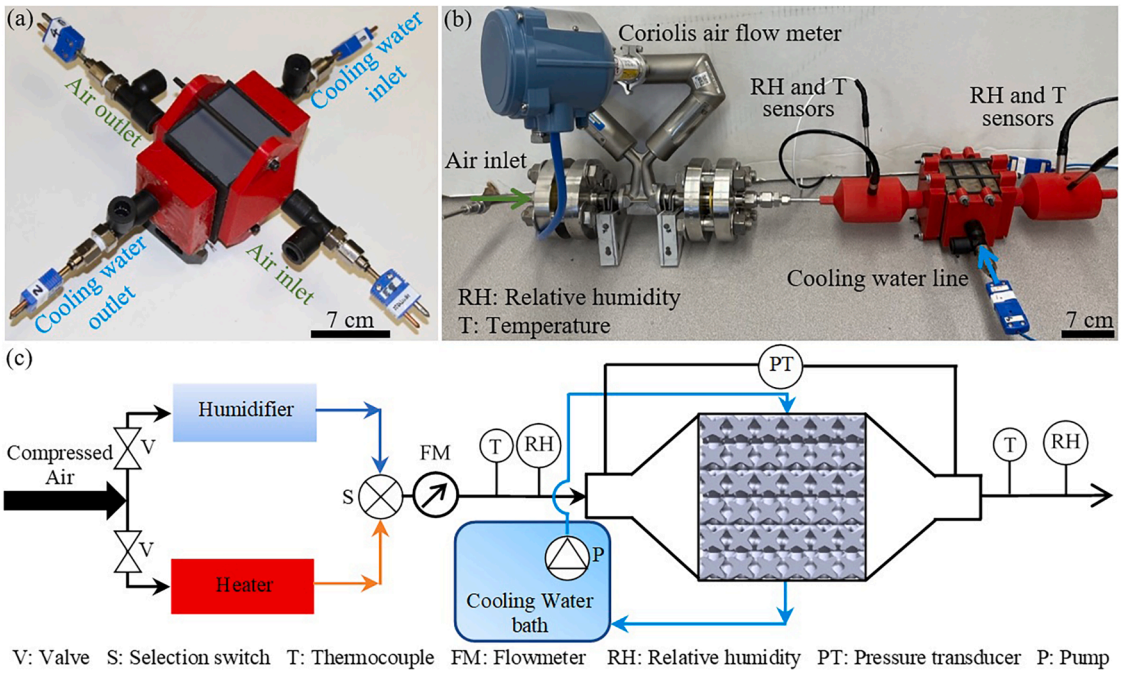

Fig. 4. (a) An image of the 3D-printed DCHX assembly, (b) an image of the dehumidification test loop facility, and (c) a schematic of the dehumidification test setup.

The dehumidification test facility is equipped with several thermocouples (Model: ReoTemp F-M12T1SU4) and an air flow meter (Model: Micro Motion ELITE CMF025H Coriolis Flow/Density Meter, Emerson Electric Co.) to measure air temperature and mass flow rate. Two warmed-probe humidity sensors (Model: HMT 337, Vaisala Inc.) provide fast and reliable humidity measurements at low to highly humid conditions. They are positioned at the inlet and outlet of the DCHX module.

4.3. Data reduction and uncertainty analysis

Moisture removal capacity (MRC) and specific cooling capacity (SCC) of the proposed lung-inspired 3D-printed DCHX are defined as follows:

$$MRC = \frac{1}{t_d}\int_0^{t_d} (\omega_{in} - \omega_{out}(t))dt[kg/kg] \tag{1}$$

$$SCC = \frac{1}{t_d}\int_0^{t_d} (h_{in} - h_{out}(t))dt[kJ/kg] \tag{2}$$

where ω_{in}, ω_{out},t_d, h_{in}, and h_{out} are inlet humidity ratio, outlet humidity ratio, adsorption period, inlet enthalpy, and outlet enthalpy, respectively.

Adsorption/regeneration rate, $\dot{m}_v$, of the lung-inspired DCHX is then defined as the net moisture exchange rate as follows:

$$\dot{m}_v = \frac{\dot{m}_a}{t_d}\int_0^{t_d} (\omega_{in} - \omega_{out}(t))dt[kg/s] \tag{3}$$

where $\dot{m}_{air}$, ω_{in}, and ω_{out} are air mass flow rate, inlet humidity ratio, and outlet humidity ratio, respectively. Volumetric adsorption rate, J, is considered to compare the performance of the proposed lung-inspired DCHX with that of existing DCHXs. The volumetric adsorption rate is defined as the adsorption rate per unit volume of the DCHX as follows:

$$J = \frac{\dot{m}_a}{t_d V}\int_0^{t_d} (\omega_{in} - \omega_{out}(t))dt[kg/m^3 - s] \tag{4}$$

where V is the volume of the DCHX module.

The coefficient of performance (COP) for the thermally-driven regeneration process is calculated as follows:

$$COP_{thermal} = \left(\frac{\dot{m}_v h_{fg}}{\dot{m}_{air} \times SCC}\right)_{regeneration} \tag{5}$$

The uncertainty associated with the MRC, and SCC are calculated as follows:

$$\frac{\delta MRC}{MRC} = \sqrt{\left(\frac{\delta\omega_{in}}{\Delta\omega}\right)^2 + \left(\frac{\delta\omega_{out}}{\Delta\omega}\right)^2} \tag{6}$$

$$\frac{\delta SCC}{SCC} = \sqrt{\left(\frac{\delta h_{in}}{\Delta h}\right)^2 + \left(\frac{\delta h_{out}}{\Delta h}\right)^2} \tag{7}$$

where $\Delta\omega$ and Δh are $(\omega_{in} - \omega_{out})$ and $(h_{in} - h_{out})$, respectively. Similarly, the uncertainty associated with the volumetric adsorption rate and COP are calculated as follows:

$$\frac{\delta J}{J} = \sqrt{\left(\frac{\delta\dot{m}_{air}}{\dot{m}_{air}}\right)^2 + \left(\frac{\delta\omega_{in}}{\Delta\omega}\right)^2 + \left(\frac{\delta\omega_{out}}{\Delta\omega}\right)^2 + \left(\frac{\delta V}{V}\right)^2} \tag{8}$$

$$\frac{\delta COP}{COP} = \sqrt{\left(\frac{\delta\dot{m}_v}{\dot{m}_v}\right)^2 + \left(\frac{\delta\dot{m}_{air}}{\dot{m}_{air}}\right)^2 + \left(\frac{\delta SCC}{SCC}\right)^2} \tag{9}$$

Table 3
Nominal value, range, accuracy, and uncertainty of main parameters.

Parameter [unit]	Nominal value	Range	Accuracy	Uncertainty
Air mass flow rate [g/s]	1.0	0.5–1.5	± 0.005	± 0.25%
Air temperature [°C]	50	30–60	± 0.5	± 1.25%
Relative humidity [%]	50	5–80	± 1	± 2%
Pressure [kPa]	2.2	0.7–4	± 0.2	± 1%
Moisture removal capacity [g/kg]	10	7–13	± 0.77	± 7.7%
Coefficient of performance	0.46	0.3–0.56	± 0.05	± 11%
Specific cooling capacity [kJ/kg]	30	22–41	± 2.3	± 7.7%
Adsorption/regeneration rate [mg/s]	10	6–13	± 0.77	± 7.7%
Volumetric adsorption rate [g/m^3-s]	43.3	26.1–54.8	± 3.6	± 8.2%

Table 3 lists nominal value, range, accuracy, and uncertainty of main experimental parameters including air volumetric flow rate, air temperature, relative humidity, pressure, adsorption/regeneration rate, and volumetric adsorption rate.

4.4. Test procedure

Adsorption tests were conducted to evaluate the dehumidification performance of the proposed lung-inspired 3D-printed DCHX module. The coated desiccant media were initially regenerated to ensure a consistent activation level before each adsorption test. An air stream at a temperature of 50 °C and a mass flow rate of 1.0 g/s was employed to regenerate the desiccant media. To study the adsorption characteristics of the proposed lung-inspired DCHX, an inlet air relative humidity level of 80% and various air mass flow rates of 0.5, 1.0, and 1.5 g/s were examined. Additionally, the heat released during the adsorption process decreases the performance of the DCHX module. One objective of the proposed lung-inspired 3D-printed DCHX is to volumetrically cool the desiccant media and further improve the adsorption process. Therefore, two series of adsorption tests without (i.e., adiabatic) and with internal cooling (i.e., diabatic) were examined.

The coated desiccant media were initially saturated to ensure a consistent thermodynamic state for the desiccant media before each regeneration test. Here, an air stream at a relative humidity of 80%, a temperature of 30 °C, and a mass flow rate of 1.0 g/s were used to saturate the desiccant media. To understand the regeneration characteristics of the proposed lung-inspired DCHX module, three inlet air temperatures of 40, 50, and 60 °C at three different air mass flow rates of 0.5, 1.0, and 1.5 g/s were investigated. Additionally, each test was repeated at least three times to ensure repeatability of the data presented.

5. Results and discussion

The dehumidification performance of the lung-inspired 3D-printed DCHX module was studied from three major perspectives: adiabatic adsorption process, diabatic adsorption process with internal cooling, and regeneration process. Additionally, the thermal energy efficiency of the lung-inspired DCHX was examined at different regeneration temperatures.

5.1. Adiabatic adsorption characteristics of the lung-inspired DCHX

Fig. 5a and b show the outlet air humidity ratio and instantaneous adsorption rate of the lung-inspired 3D-printed DCHX versus time at two different air mass flow rates of 0.5 and 1.5 g/s during the adsorption process. The inlet air relative humidity, temperature, and humidity ratio were fixed at 80%, 30 °C, and 21.6 g/kg, respectively. Before each adsorption test, the desiccant media was first activated by a hot air stream at a temperature of 50 °C. As evident, the lung-inspired DCHX demonstrates a promising potential in dehumidifying the inlet humid air stream and delivering a relatively dry air condition. At a fixed air mass flow rate, the outlet humidity ratio increases with time. This is attributed to the water vapor pressure potential, which decreases as water vapor molecules are adsorbed at the desiccant-air interface during the dehumidification process. This subsequently decreases the instantaneous adsorption rate as shown in Fig. 5b, thereby increasing the outlet air humidity ratio with time. Additionally, the instantaneous adsorption rate increases at higher air mass flow rates as shown in Fig. 5b. For instance, the time-averaged adsorption rate of the lung-inspired 3D-printed DCHX is 11.4 mg/s at an air mass flow rate of 1.5 g/s, which is a 90% improvement compared with an adsorption rate of 6.0 mg/s at an air mass flow rate of 0.5 g/s. This is because the mass transfer boundary layer thickness shrinks at higher air mass flow rates, thereby increasing the overall adsorption rate. This also leads to a rapid rise in the outlet air humidity ratio with time at higher mass flow rates as shown in Fig. 5a. At higher adsorption rates, the desiccant media get saturated more quickly, thereby increasing the outlet air humidity ratio.

5.2. Diabatic adsorption characteristics of the lung-inspired DCHX

The equilibrium water vapor pressure at the desiccant-air interface is reduced if the desiccant media is simultaneously cooled during the adsorption process. This subsequently improves the adsorption performance. The proposed lung-inspired 3D-printed DCHX volumetrically distributes a cooling water stream within and through the desiccant media, thereby facilitating rejection of the heat released during the adsorption process. Fig. 6 shows variations of the outlet air humidity ratio and corresponding instantaneous adsorption rate versus time at three different air mass flow rates of 0.5, 1, and 1.5 g/s during adiabatic (i.e., no internal cooling) and diabatic (i.e., with internal cooling) adsorption processes. The inlet temperature of the cooling water stream was constant at 18 °C. As evident, the outlet air humidity ratio of the diabatic adsorption process is lower than that of the adiabatic adsorption process at all air mass flow rates examined. In other words, a higher humidity content is captured when the desiccant-coated layer is cooled. This is clearly illustrated in Fig. 7 in which the instantaneous adsorption rate of the diabatic adsorption process is higher than that of the adiabatic adsorption process at all air mass flow rates. For instance, at an air mass flow rate of 1.5 g/s, the time-averaged adsorption rate of the

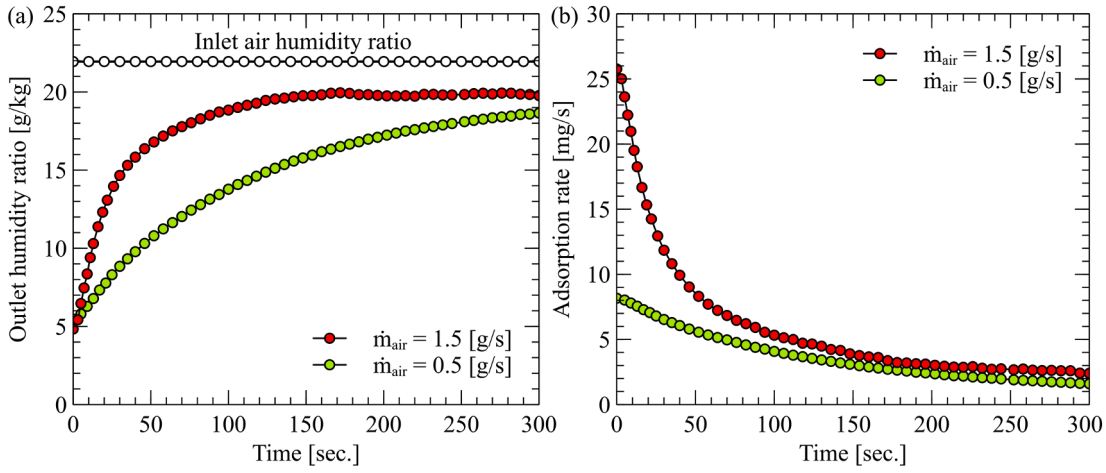

Fig. 5. Variations of the (a) outlet air humidity ratio, and (b) instantaneous adsorption rate versus time at two different air mass flow rates of 0.5 and 1.5 g/s during the adsorption process.

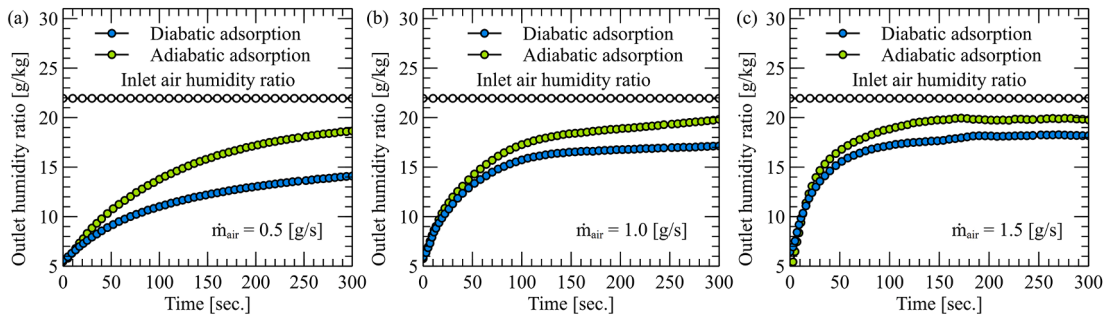

Fig. 6. Variations of the outlet air humidity ratio versus time at three air mass flow rates of (a) 0.5, (b) 1.0, and (c) 1.5 g/s during adiabatic (i.e., no internal cooling) and diabatic (i.e., with internal cooling) adsorption processes.

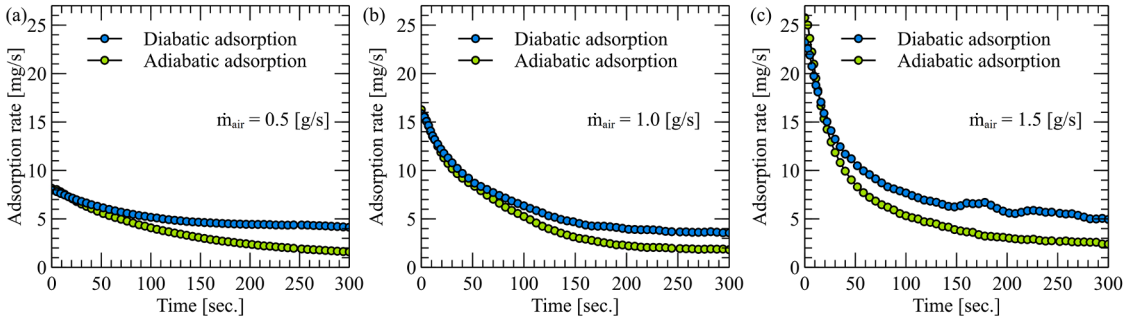

Fig. 7. Variations of the instantaneous adsorption rate versus time at three different air mass flow rates of (a) 0.5, (b) 1.0, and (c) 1.5 g/s during adiabatic and diabatic adsorption processes.

diabatic adsorption process is 12.6 mg/s, an 11% improvement compared with that of the adiabatic adsorption process.

Fig. 8 shows variations of the time-averaged volumetric adsorption rate, moisture removal capacity (MRC), and specific cooling capacity (SCC) as a function of mass flow rate for the diabatic and adiabatic adsorption processes. The volumetric adsorption rate, MRC, and SCC of the diabatic adsorption process exceed those of the adiabatic adsorption process due to a lower equilibrium water vapor pressure of the cooled desiccant media. As expected and shown in Fig. 8a, the volumetric adsorption rate increases with the air mass flow rate due to an enhanced convective mass transfer process. Fig. 8a also shows that the MRC decreases with the mass flow rate. For instance, the diabatic MRC decreases from 12.9 to 8.4 g/kg when the air mass flow rate increases from 0.5 to 1.5 g/s. The MRC is directly proportional to the adsorption rate and inversely related to the air mass flow rate. Although the adsorption rate increases with the air mass flow rate, its effect on the MRC is more pronounced, thereby decreasing the MRC at higher air mass flow rates. Additionally, Fig. 8b shows that the SCC decreases with the air mass flow rate. In other words, the outlet air enthalpy is closer to the inlet air enthalpy at higher air mass flow rates. For instance, the diabatic SCC decreases from 40.6 to 27.4 kJ/kg when the air mass flow rate increases from 0.5 to 1.5 g/s.

5.3. Regeneration characteristics of the lung-inspired DCHX

The water vapor molecules adsorbed onto the surface of the desiccant-coated layer need to be rejected to recover its water vapor uptake capacity. This is accomplished by the regeneration process in

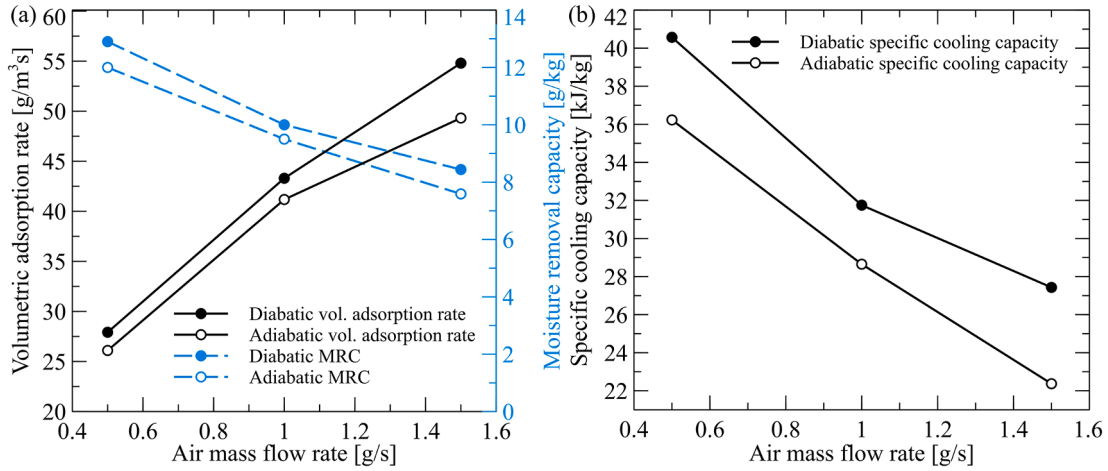

Fig. 8. Variations of the time-averaged (a) moisture removal capacity and volumetric adsorption rate, and (b) specific cooling capacity versus air mass flow rate during diabatic and adiabatic adsorption processes.

which a hot air stream heats the desiccant-coated layer increasing its equilibrium water vapor pressure at the desiccant-air interface, thereby facilitating the regeneration process. Fig. 9 shows the outlet air humidity ratio and instantaneous regeneration rate of the lung-inspired 3D-printed DCHX versus time at two different air mass flow rates of 0.5 and 1.5 g/s during the regeneration process. The inlet temperature of the air stream was fixed at 50 °C. Before each regeneration test, the desiccant media was first saturated using a humid air stream at a relative humidity of 80%, a temperature of 30 °C, and a mass flow rate of 1 g/s. At a fixed air mass flow rate, the outlet air humidity ratio decreases with time. This is because the available water vapor pressure potential for the regeneration process decreases as the previously adsorbed water vapor molecules are rejected at the desiccant-air interface. This leads to a reduction in the instantaneous regeneration rate as shown in Fig. 9b, thereby reducing the outlet humidity ratio with time. Additionally, the instantaneous regeneration rate increases at higher air mass flow rates as shown in Fig. 9b. For example, the time-averaged regeneration rate of the lung-inspired 3D-printed DCHX improves from 4.8 to 9.4 mg/s (i.e., a 96% enhancement) when the air mass flow rate increases from 0.5 to 1.5 g/s. This is because the mass transfer coefficient increases at higher air flow rates due to a reduced mass boundary layer thickness, thereby increasing the regeneration rate. This also results in a rapid drop in the outlet air humidity ratio with time at higher mass flow rates as shown in Fig. 8a.

Fig. 10 shows the effect of the air inlet temperature on the thermal COP of the regeneration process at an air inlet mass flow rate of 0.5 g/s. As evident, the thermal energy efficiency of the regeneration process decreases with the air inlet temperature. For instance, the thermal COP of the regeneration process decreases from 0.56 to 0.3 when the air inlet temperature increases from 40 to 60 °C. This can be attributed to the water vapor pressure of the air and desiccant media and the time scales of the regeneration cycle and convective heat transfer process. At higher air inlet temperatures, the partial water vapor pressure of the air is higher. However, at short regeneration cycles, the desiccant media might not have enough time to fully sense the higher air temperature and thus increase its water vapor pressure for the regeneration process. In other words, at short regeneration cycles and higher air inlet temperatures, a larger part of the sensible heat carried by the hot stream leaves the system before being involved in the regeneration process. The result is a drop in thermal COP with the air inlet temperature as shown in Fig. 10.

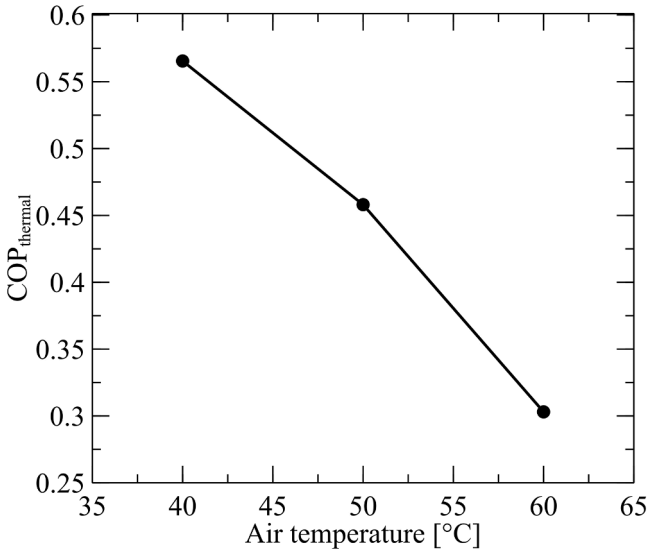

Fig. 10. Variations of COP at different air regeneration temperatures.

5.4. Comparison against existing solid-desiccant-based dehumidification technologies

Fig. 11 compares the volumetric adsorption rate of several existing solid-desiccant-based dehumidification technologies as a function of their associated air pressure drop penalties. A system with a high volumetric adsorption rate and a low pressure drop penalty is desirable. As it can be seen, a fluidized bed dehumidification system developed by Chen et al. [15] showed a maximum volumetric adsorption rate of about 0.84 g/m^3-s at a pressure drop penalty of around 4 kPa. A circulating fluidized bed system developed by Chiang et al. [16] revealed a maximum volumetric adsorption rate of approximately 1.4 g/m^3-s at a pressure drop penalty of around 1.3 kPa, a performance improvement over standard fluidized bed systems. Rotary wheel desiccant dehumidification systems demonstrate a notable volumetric adsorption rate of about 6.75 g/m^3-s at a low pressure drop penalty of around 0.2 kPa [36]. A desiccant packed heat exchanger developed by Mohammed et al. [34] exhibited a high volumetric adsorption rate of approximately 22 g/m^3-s at an estimated pressure drop penalty of around 1 kPa. The proposed lung-inspired 3D-printed DCHX design offers an excellent balance between a remarkable volumetric adsorption rate and a low pressure drop penalty. At the highest air mass flow rate examined (i.e., 1.5 g/s), the

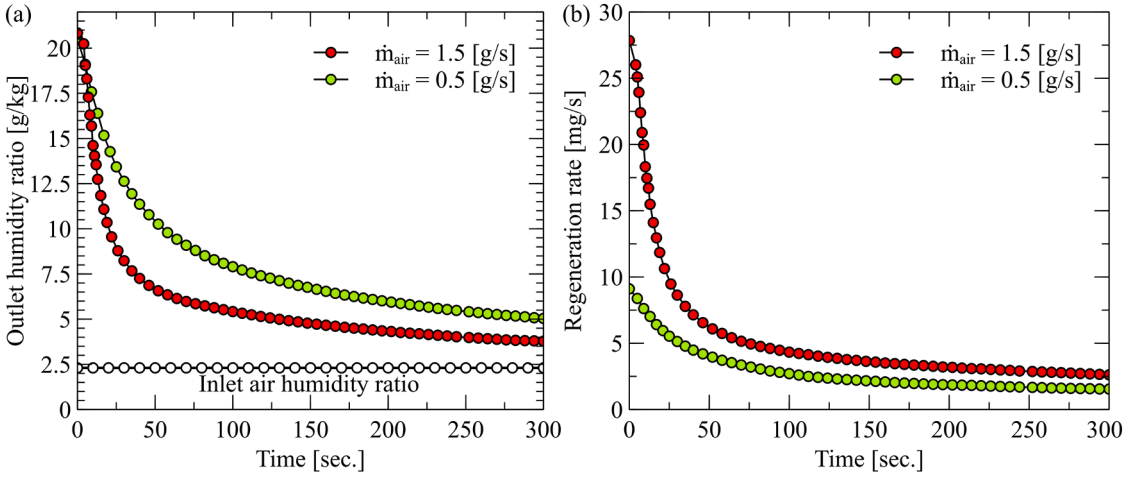

Fig. 9. Variations of the (a) outlet air humidity ratio, and (b) instantaneous regeneration rate versus time at two different air mass flow rates of 0.5 and 1.5 g/s during the regeneration process.

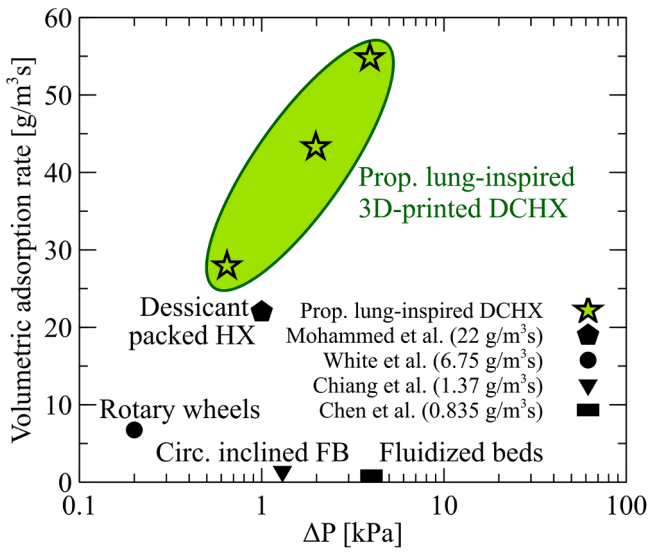

Fig. 11. Volumetric adsorption rate of various solid-desiccant-based dehumidification systems as a function of their associated air pressure drop penalties.

volumetric adsorption rate and pressure drop penalty values of the proposed DCHX technology are 54.8 g/m^3-s and 4 kPa, respectively. This signifies that the lung-inspired 3D-printed DCHX significantly outperforms existing solid-desiccant-based dehumidification technologies.

6. Conclusion

In summary, this study introduced an innovative 3D-printed DCHX concept inspired by the bronchi arrangement of a human lung to address the shortcomings of standard DCHX designs. The lung-inspired DCHX employs two intertwined bicontinuous flow networks ensuring a volumetric distribution of one fluid network within and through the other network. This results in highly efficient heat and mass transfer characteristics for augmented adsorption and regeneration processes at low pressure drop penalties.

Various factors affecting the adiabatic/diabatic adsorption, regeneration, MRC, SCC, and thermal energy efficiency characteristics of the proposed lung-inspired 3D-printed DCHX were experimentally examined. The main concluding remarks of the present study are:

- The transient and time-averaged adiabatic/diabatic volumetric adsorption rates of the lung-inspired 3D-printed DCHX increase with the air mass flow rate.
- The volumetric adsorption rate of the diabatic process is higher than that of the adiabatic process. The diabatic volumetric adsorption rate is 54.8 g/m^3-s, which is an 11% improvement compared with an adiabatic volumetric adsorption rate of 49.3 g/m^3-s at an air inlet mass flow rate of 1.5 g/s.
- The time-averaged adiabatic/diabatic MRC and SCC values decrease with the air mass flow rate. The diabatic MRC decreases from 12.9 to 8.4 g/kg when the air mass flow rate increases from 0.5 to 1.5 g/s. The diabatic SCC decreases from 40.6 to 27.4 kJ/kg when the air mass flow rate increases from 0.5 to 1.5 g/s.
- The transient and time-averaged regeneration rates of the lung-inspired 3D-printed DCHX increase at higher air mass flow rates. At an air inlet temperature of 50 °C, the time-averaged regeneration rate increases from 4.8 to 9.4 mg/s (i.e., a 96% enhancement) when the air mass flow rate increases from 0.5 to 1.5 g/s.
- The proposed lung-inspired DCHX technology outperforms state-of-the-art DCHX systems by offering a high volumetric adsorption rate of 54.8 g/m^3-s at a low pressure drop penalty of 4 kPa.

The experimental results presented here demonstrate the promising potential of the lung-inspired 3D-printed DCHX concept for a wide range of applications including desiccant-based air conditioning and drying systems. It is envisioned that these systems employ two lung-inspired DCHX modules for the adsorption and regeneration processes, thereby allowing a continuous dehumidification operation. Future works will focus on performance evaluation and optimization of the proposed lung-inspired DCHX technology at the system level incorporating both adsorption and regeneration processes simultaneously. Additionally, adsorption and regeneration performances of the lung-inspired DCHX concept with emerging solid desiccants including metal–organic frameworks (MOFs) will be examined.

CRediT authorship contribution statement

Umamaheswar Puttur: Investigation, Visualization, Writing – original draft. **Masoud Ahmadi:** Investigation, Data curation, Visualization, Writing – original draft. **Behzad Ahmadi:** Investigation, Writing – original draft. **Sajjad Bigham:** Conceptualization, Supervision, Methodology, Writing – original draft, Writing – review & editing.

Declaration of Competing Interest

The authors declare that they have no known competing financial interests or personal relationships that could have appeared to influence the work reported in this paper.

Acknowledgments

This study was sponsored by the U.S. Department of Energy's Office of Energy Efficiency and Renewable Energy (EERE) under the Building Technology Office Award Number DE-EE0008685. The authors would like to acknowledge Mr. Antonio Bouza and Mr. Mohammed Khan, Technology Managers, and Mr. Michael Geocaris, and Mr. Andrew Kobusch, Project Engineers, HVAC, Water Heating, and Appliance subprogram, Building Technologies Office, the U.S. Department of Energy.

References

[1] Harriman LG, Plager D, Kosar D. Dehumidification and cooling loads from ventilation air. Energy Eng J Assoc Energy Eng 1999;96:31–45. https://doi.org/10.1080/01998595.1999.10530479.
[2] Harriman LG. The dehumidification handbook; 2002.
[3] Yeboah SK, Darkwa J. A critical review of thermal enhancement of packed beds for water vapour adsorption. Renew Sustain Energy Rev 2016;58:1500–20. https://doi.org/10.1016/j.rser.2015.12.134.
[4] Sen Chang K, Wang HC, Chung TW. Effect of regeneration conditions on the adsorption dehumidification process in packed silica gel beds. Appl Therm Eng 2004;24:735–42. https://doi.org/10.1016/j.applthermaleng.2003.11.003.
[5] Pesaran A. A review of desiccant dehumidification technology. ERPI's Electr Dehumidification Energy Effic Humidity Control Commer Industitutional Build Conf; 1993.
[6] Shamim JA, Hsu WL, Kitaoka K, Paul S, Daiguji H. Design and performance evaluation of a multilayer fixed-bed binder-free desiccant dehumidifier for hybrid air-conditioning systems: Part I – experimental. Int J Heat Mass Transf 2018;116:1361–9. https://doi.org/10.1016/j.ijheatmasstransfer.2017.09.051.
[7] Harshe YM, Utikar RP, Ranade VV, Pahwa D. Modeling of rotary desiccant wheels. Chem Eng Technol 2005;28:1473–9. https://doi.org/10.1002/ceat.200500164.
[8] Zhou X, Reece R. Experimental investigation for a non-adiabatic desiccant wheel with a concentric structure at low regeneration temperatures. Energy Convers Manag 2019;201:112165. https://doi.org/10.1016/j.enconman.2019.112165.
[9] Goldsworthy M, White SD. Limiting performance mechanisms in desiccant wheel dehumidification. Appl Therm Eng 2012;44:21–8. https://doi.org/10.1016/j.applthermaleng.2012.03.046.
[10] Goodarzia G, Thirukonda N, Heidari S, Akbarzadeh A, Date A. Performance Evaluation of Solid Desiccant Wheel Regenerated by Waste Heat or Renewable Energy. Energy Procedia 2017;110:434–9. https://doi.org/10.1016/j.egypro.2017.03.165.

[11] Kang H, Lee DY. Experimental investigation and introduction of a similarity parameter for characterizing the heat and mass transfer in polymer desiccant wheels. Energy 2017;120:705–17. https://doi.org/10.1016/j.energy.2016.11.122.
[12] Bourdoukan P, Wurtz E, Joubert P. Comparison between the conventional and recirculation modes in desiccant cooling cycles and deriving critical efficiencies of components. Energy 2010;35:1057–67. https://doi.org/10.1016/j.energy.2009.06.021.
[13] Kanoğlu M, Çarpinlioğlu MÖ, Yildirim M. Energy and exergy analyses of an experimental open-cycle desiccant cooling system. Appl Therm Eng 2004;24:919–32. https://doi.org/10.1016/j.applthermaleng.2003.10.003.
[14] Kang H, Lee G, Lee DY. Explicit analytic solution for heat and mass transfer in a desiccant wheel using a simplified model. Energy 2015;93:2559–67. https://doi.org/10.1016/j.energy.2015.10.091.
[15] Chen CH, Ma SS, Wu PH, Chiang YC, Chen SL. Adsorption and desorption of silica gel circulating fluidized beds for air conditioning systems. Appl Energy 2015;155:708–18. https://doi.org/10.1016/j.apenergy.2015.06.041.
[16] Chiang YC, Chen CH, Chiang YC, Chen SL. Circulating inclined fluidized beds with application for desiccant dehumidification systems. Appl Energy 2016;175:199–211. https://doi.org/10.1016/j.apenergy.2016.05.009.
[17] Hua LJ, Ge TS, Wang RZ. A mathematical model to predict the performance of desiccant coated evaporators and condensers. Int J Refrig 2020;109:188–207. https://doi.org/10.1016/j.ijrefrig.2019.10.001.
[18] Sun XY, Dai YJ, Ge TS, Zhao Y, Wang RZ. Comparison of performance characteristics of desiccant coated air-water heat exchanger with conventional air-water heat exchanger – Experimental and analytical investigation. Energy 2017;137:399–411. https://doi.org/10.1016/j.energy.2017.03.078.
[19] Zhao Y, Dai YJ, Ge TS, Wang HH, Wang RZ. A high performance desiccant dehumidification unit using solid desiccant coated heat exchanger with heat recovery. Energy Build 2016;116:583–92. https://doi.org/10.1016/j.enbuild.2016.01.021.
[20] Vivekh P, Bui DT, Kumja M, Islam MR, Chua KJ. Theoretical performance analysis of silica gel and composite polymer desiccant coated heat exchangers based on a CFD approach. Energy Convers Manag 2019;187:423–6. https://doi.org/10.1016/j.enconman.2019.02.093.
[21] Hua LJ, Sun XY, Jiang Y, Ge TS, Wang RZ. Graphic general solutions for desiccant coated heat exchangers based on dimensional analysis. Int J Heat Mass Transf 2020;154:19–22. https://doi.org/10.1016/j.ijheatmasstransfer.2020.119654.
[22] Tu YD, Wang RZ, Hua LJ, Ge TS, Cao BY. Desiccant-coated water-sorbing heat exchanger: Weakly-coupled heat and mass transfer. Int J Heat Mass Transf 2017;113:22–31. https://doi.org/10.1016/j.ijheatmasstransfer.2017.05.047.
[23] Vivekh P, Islam MR, Chua KJ. Experimental performance evaluation of a composite superabsorbent polymer coated heat exchanger based air dehumidification system. Appl Energy 2020;260:114256. https://doi.org/10.1016/j.apenergy.2019.114256.
[24] Vivekh P, Bui DT, Wong Y, Kumja M, Chua KJ. Performance evaluation of PVA-LiCl coated heat exchangers for next-generation of energy-efficient dehumidification. Appl Energy 2019;237:733–50. https://doi.org/10.1016/j.apenergy.2019.01.018.
[25] Zheng X, Wang R, Ma W. Dehumidification assessment for desiccant coated heat exchanger systems in different buildings and climates: Fast choice of desiccants. Energy Build 2020;221:110083. https://doi.org/10.1016/j.enbuild.2020.110083.
[26] Li A, Thu K, Bin Ismail A, Shahzad MW, Ng KC. Performance of adsorbent-embedded heat exchangers using binder-coating method. Int. J Heat Mass Transf 2016;92:149–57. https://doi.org/10.1016/j.ijheatmasstransfer.2015.08.097.
[27] Zhao Y, Ge TS, Dai YJ, Wang RZ. Experimental investigation on a desiccant dehumidification unit using fin-tube heat exchanger with silica gel coating. Appl Therm Eng 2014;63:52–8. https://doi.org/10.1016/j.applthermaleng.2013.10.018.
[28] Amani M, Bahrami M. Greenhouse dehumidification by zeolite-based desiccant coated heat exchanger. Appl Therm Eng 2021;183:116178. https://doi.org/10.1016/j.applthermaleng.2020.116178.
[29] Ge TS, Zhang JY, Dai YJ, Wang RZ. Experimental study on performance of silica gel and potassium formate composite desiccant coated heat exchanger. Energy 2017;141:149–58. https://doi.org/10.1016/j.energy.2017.09.090.
[30] Erkek TU, Gungor A, Fugmann H, Morgenstern A, Bongs C. Performance evaluation of a desiccant coated heat exchanger with two different desiccant materials. Appl Therm Eng 2018;143:701–10. https://doi.org/10.1016/j.applthermaleng.2018.06.012.
[31] Oh SJ, Ng KC, Chun W, Chua KJE. Evaluation of a dehumidifier with adsorbent coated heat exchangers for tropical climate operations. Energy 2017;137:441–8. https://doi.org/10.1016/j.energy.2017.02.169.
[32] Vivekh P, Kumja M, Bui DT, Chua KJ. Recent developments in solid desiccant coated heat exchangers – A review. Appl Energy 2018;229:778–803. https://doi.org/10.1016/j.apenergy.2018.08.041.
[33] Vivekh P, Bui DT, Islam MR, Zaw K, Chua KJ. Experimental performance and energy efficiency investigation of composite superabsorbent polymer and potassium formate coated heat exchangers. Appl Energy 2020;275:115428. https://doi.org/10.1016/j.apenergy.2020.115428.
[34] Mohammed RH, Mesalhy O, Elsayed ML, Huo R, Su M, Chow LC. Performance of desiccant heat exchangers with aluminum foam coated or packed with silica gel. Appl Therm Eng 2020;166:114626. https://doi.org/10.1016/j.applthermaleng.2019.114626.
[35] Wang C, Ji X, Yang B, Zhang R, Yang D. Study on heat transfer and dehumidification performance of desiccant coated microchannel heat exchanger. Appl Therm Eng 2021;192. https://doi.org/10.1016/j.applthermaleng.2021.116913.
[36] White SD, Goldsworthy M, Reece R, Spillmann T, Gorur A, Lee DY. Characterization of desiccant wheels with alternative materials at low regeneration temperatures. Int J Refrig 2011;34:1786–91. https://doi.org/10.1016/j.ijrefrig.2011.06.012.
[37] Ahmadi B, Ahmadi M, Nawaz K, M. Momen A, Bigham S. Performance analysis and limiting parameters of cross-flow membrane-based liquid-desiccant air dehumidifiers. Int J Refrig 2021. https://doi.org/10.1016/j.ijrefrig.2021.09.010. In press.
[38] Ahmadi M, R. Gluesenkamp K, Bigham S. Energy-efficient sorption-based gas clothes dryer systems. Energy Convers Manage 2021;230. https://doi.org/10.1016/j.enconman.2020.113763.
[39] Pinnu S, Bigham S. Multiple-effect desiccant-based zero liquid discharge desalination systems. Desalination 2021;502. https://doi.org/10.1016/j.desal.2021.114942.